JOURNAL OF CATALYSIS 90, 40–48 (1984)

Nickel Crystallite Thermometry during Ethane Hydrogenolysis

T. S. CALE

Department of Chemical Engineering, Arizona State University, Tempe, Arizona 85287

Received February 16, 1984; revised June 25, 1984

A magnetic method to measure the average temperature of superparamagnetic nickel crystallites during ethane hydrogenolysis over Ni/SiO_2 is detailed. The method uses the temperature dependence of the magnetic moment per unit volume of crystallite for nickel, which is determined from the low magnetic field sample moment measured with an ac permeameter. Small corrections for hydrogen partial pressure changes are required. Two applications of this catalytic crystallite thermometry are discussed: (1) kinetics in the presence of external temperature gradients, and (2) interphase heat transfer experiments. © 1984 Academic Press, Inc.

INTRODUCTION

Perhaps the best measure of reaction temperature during supported metal catalysis is the temperature of the metal crystallites. The temperature of supported metal crystallites has been the subject of several analytical studies (*1–6*). Large, rapid thermal excursions have been predicted to explain sintering of supported metal crystallites during exothermic reaction (*1–3*). Of more use in heterogeneous kinetic data analysis is the time average crystallite temperature, which is predicted to be very close to that of the support (*6*). However, there has been no quantitative thermometric method available to verify this last statement.

A magnetic method to measure the average nickel crystallite temperature during ethane hydrogenolysis has been introduced (*7*). The reasons for selecting this system are detailed there. Essentially, the system was selected because of (*1*) its relatively simple magnetochemistry and (*2*) the magnetic moment density of nickel is temperature sensitive in a range where its hydrogenolysis activity is reasonable (500–550 K). The major result reported in Ref. (*7*) is that the average crystallite temperature is reasonably close to the local bed average for reasonable reaction rates, in agreement with prediction. This paper presents the details of the crystallite thermometry as currently performed, and discusses early results of two applications.

The basis for the thermometry is the temperature dependence of magnetic moment density (moment per unit volume of magnetic material) for superparamagnetic samples (*7*). This is often referred to as spontaneous magnetization (*8*) since the superparamagnetic samples are composed of single-domain crystallites of ferromagnetic materials, such as nickel. As there is nothing spontaneous about the net magnetization of superparamagnetic samples, moment density will be used in this paper. Note that it is the magnetization, or moment density, of individual nickel domains which is of interest. Cale (*9*) has extended classical superparamagnetic superposition analysis (*8*) to determine magnetic phase composition in $NiCu/SiO_2$ catalysts (*10*) and to demonstrate a crystallite size dependence of the magnetic moment density for Ni/SiO_2 (*11*). This concept is employed in magnetic thermometry, where it is sufficient and convenient to concentrate on the low magnetic field behavior of these samples (*9–11*). The low field (H) magnetic moment (M_{LF}) of a superparamagnetic specimen relative to its saturation moment (M_∞) at a given temperature (T) is (*8*)

0021-9517/84 $3.00
Copyright © 1984 by Academic Press, Inc.
All rights of reproduction in any form reserved.

$$\frac{M_{LF}(T)}{M_\infty(T)} = \frac{M_{LF}(T)}{VI_s(T)} = \frac{I_s \upsilon H}{3kT} \qquad (1)$$

where

V is total volume of magnetic material,
υ is average crystallite volume,
k is Boltzmann's constant,
I_s is the moment density of the magnetic material.

This can be used to determine the temperature dependence of magnetic moment density. For a given sample at a fixed field, Eq. (1) can be used to show that

$$\frac{I_s(T)}{I_s(T_R)} = \left[\frac{TM_{LF}(T)}{T_R M_{LF}(T_R)}\right]^{1/2} \qquad (2)$$

where T_R is some reference temperature.

Figure 1, taken from Ref. (*11*), shows the temperature dependence of magnetic moment density as $I_s(T)/I_s$ (0 K) for two Ni/SiO_2 samples with different average crystallite sizes. The data was taken using a Princeton Applied Research vibrating sample magnetometer. The sizes are given as the spherical radius corresponding to the average volume determined from low field magnetization data (*8*). An intrinsic crystallite size effect is clear, so the temperature dependence of magnetic moment density will differ between samples, in general. The

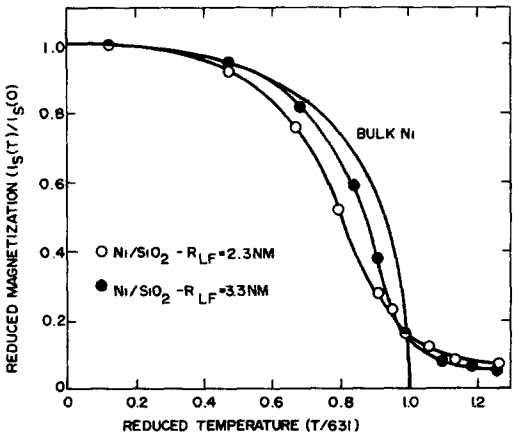

FIG. 1. Reduced magnetic moment per unit nickel volume as a function of reduced temperature. R_{LF} is the radius calculated from the first volume moment determined from low field magnetization.

sample temperature can readily be determined from the sample moment at that temperature relative to the sample moment at the reference temperature. Equation (2) is applied, and reference is made to the $I_s(T)/I_s(T_R)$ vs temperature curve for the sample being studied (*7*). This is the essence of the magnetic thermometry, ignoring the effects of coverage on sample moment (*8*) and assuming that crystallite temperature is not a function of size.

The ac permeameter, popularized by Selwood (*8*), is a powerful and versatile tool to monitor changes in the low field sample moment of superparamagnetic samples. The net output voltage (E) of an ac permeameter varies linearly with the magnetic moment of the sample within it (*8*):

$$E_s = E - E_0 = C \cdot M_{LF}(T) \qquad (3)$$

where

C is an empirical calibration constant (mV/Oe · cm^3)
E is total output voltage of permeameter
E_s is output voltage due to the sample
E_0 is output voltage with no sample.

The empirical proportionality constant must be determined for each set of experimental parameters. The average crystallite temperature could then be determined by converting E_s (referred to as sample voltage in the following) to magnetic moment before referring to the magnetic moment density vs temperature curve for the sample.

Alternatively, one can arrive at the temperature dependence of magnetic moment density directly without evaluating the constant, by using the ratio of sample voltages at different temperatures (*8*):

$$\frac{I_s(T)}{I_s(T_R)} = \left[\frac{E_s(T)T}{E_s(T_R)T_R}\right]^{1/2} \qquad (4)$$

This is a convenient method to arrive at arbitrary portions of curves such as those in Fig. 1. Again, this considers only clean nickel crystallites.

It is equally as viable, and much easier, to develop a relationship between sample

voltage and sample temperature directly. As with other thermometries, the conversion to the actual thermometric measure (e.g., volume of mercury) is not necessary or desirable. Thus, units of magnetism are not used in the following. Given the ac permeameter output voltage for a sample with a E_s vs temperature curve available for it, the temperature can be read directly. This can be used for any superparamagnetic specimen, as long as coverage effects are not involved in the thermometry. Coverage effects are very specific to the system being studied, and will be discussed for ethane hydrogenolysis over nickel in a later section.

EXPERIMENTAL

Catalyst preparation. The Ni/SiO_2 catalyst was prepared by homogeneous precipitation–deposition using urea (*12*), a technique known to give very uniform catalysts (*13, 14*). The final catalyst, 25% Ni on Baker Analyzed Reagent grade silica gel, was sieved into fractions. The work reported here was on a 80/100 mesh sieve cut, and the average catalyst particle size is 0.16 mm.

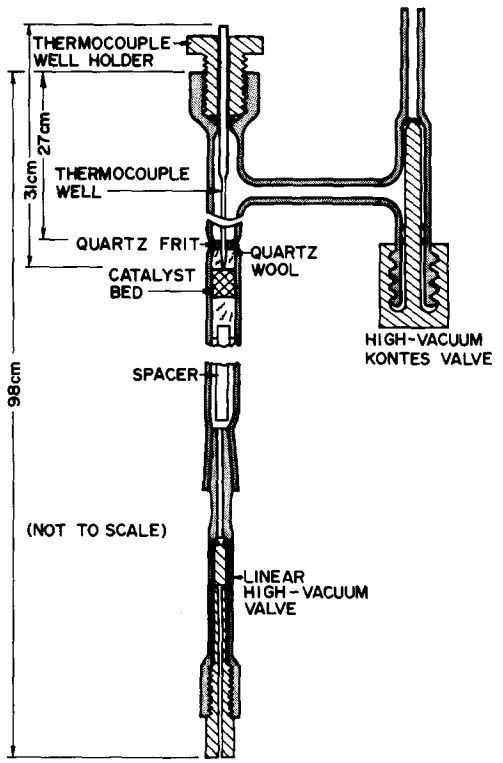

FIG. 2. Quartz sample cell/reactor for characterizations and hydrogenolysis/thermometry.

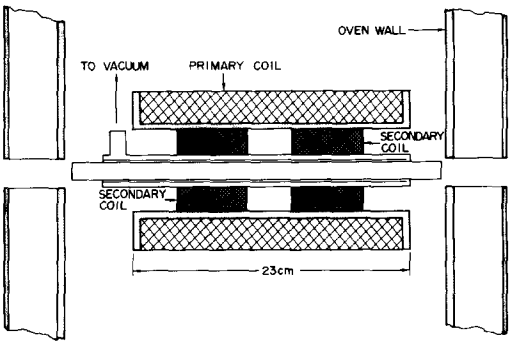

FIG. 3. Dual secondary coil ac permeameter with vacuum shields.

In situ sample cell. Figure 2 shows the quartz reactor/sample cell, similar to that of Cale and Richardson (*10*), used in the Ni crystallite thermometry. This flow cell allows for detailed *in situ* adsorptive and magnetic characterizations of the same catalyst sample used in the thermometry (*10*). A quartz thermocouple well allows measurement of the stream temperature exiting the catalyst bed.

Alternating current (ac) permeameter. Figure 3 is a schematic of the permeameter used. The primary consists of 2600 turns of 16 gauge, Allex (*15*) coated magnet wire. The two secondary coils consist of 10,500 turns each of 28 gauge Allex coated magnet wire. The outputs of the secondary coils are connected in opposition in order to minimize noise (*8, 16*). The coils are not exactly matched, so there is some output voltage in the absence of sample. This does not interfere with the experiments.

The permeameter has been operated up to 535 K, but is limited in temperature by the coating on the magnet wire. Typical operating temperatures are 500 to 520 K. This is a good temperature range for nickel crystallite thermometry during ethane hydrogenolysis as the moment density of Ni is

temperature sensitive in this range (see Fig. 1). Higher temperatures would be desired if cobalt or iron catalysts were to be used, as their Curie transitions in the bulk are at higher temperatures (*8*).

The primary coil, which has a dc resistance of 10.5 ohm at 520 K, is excited by 20 V(ac) at 50 Hz using an Elgar Model 251 power supply. This frequency is low enough for superparamagnetic behavior of the samples studied, as the average crystallite has an equivalent spherical radius of around 3 nm (*8*). The net output of the secondary coils is read on a Keithley Model 177 DMM. The dc output of this is recorded on strip chart after zeroing with a dc power supply. This balancing allows small variations in large signals to be resolved.

Sensitivity depends on coil design, primary excitation voltage, and average crystallite size in the sample. For one sample, with an average crystallite size of about 3 nm, the response was roughly 50 mV/g of Ni with the operating conditions noted. A better estimate of sensitivity is not needed, as a calibration curve is taken for each sample and this measure of sensitivity varies with sample. For the same experimental arrangement, the noise level was less than 0.005 mV. For this same sample, the voltage vs temperature curve was very linear over the range from 500 to 520 K, with a slope of 0.012 mV/K.

A unique feature of the permeameter represented in Figure 3 is the vacuum jackets surrounding the core. These are intended to shield the secondary coils from the thermal effects of reaction. If the secondary coils adsorb heat, their output changes. Comparison with unshielded secondaries is underway; however, thermal drift is sometimes apparent starting several minutes after an increase in reaction rate, hence heat release.

Kinetic apparatus. The quartz reactor used in the differential ethane hydrogenolysis/magnetic thermometry experiments has already been discussed. Mass flowmeters (Linde FM4570 with sensors) monitor the flow of hydrogen and ethane, while a rotameter is used for helium flow. Pressure is measured upstream and downstream of the reactor. The fluid temperature is measured using a thermocouple (Type K) in the well provided in the sample cell/reactor of Fig. 2, and read on an Omega Model 2176A digital readout. Ethane conversions are kept low to justify the differential reactor approximation. A Varian 1200 GC/FID is used for product analysis. Analysis is very rapid, requiring 3 min.

A unique feature of the equipment is that the inlet line can be purged and evacuated. This is necessary, since the sample cell/reactor containing the sample must be inserted in the kinetic flow stream after reduction, cleaning, and any characterizations. The constancy of sample moment upon introduction of helium flow after cyclic purging and evacuation validates the procedure used.

Sample preparation. After the sample cell is loaded with about 0.5 g of catalyst, reduction is performed in flowing hydrogen (60 cm^3/min) at 623 K. Cleaning is at 673 K in flowing helium (60 cm^3/min). High-purity hydrogen 99.997% passes through an oxygen purifier and a silica-gel trap before contacting the catalyst sample. The 99.997% helium passes through a copper oxygen scrubber, then silica gel, before contacting the sample. After reduction and cleaning, the sample is sealed in helium and removed from the reduction furnace.

NICKEL CRYSTALLITE THERMOMETRY

To begin the hydrogenolysis/thermometry experiments, the catalyst sample is centered in one of the secondary coils of the ac permeameter. The reactor is then connected to the kinetic flow system, and a flow of helium established. The permeameter output drops by about 15% upon switching from helium to hydrogen, as expected for these samples (*8, 10, 17*).

Catalytic crystallite thermometry is currently performed by following the permeameter output voltage after introducing

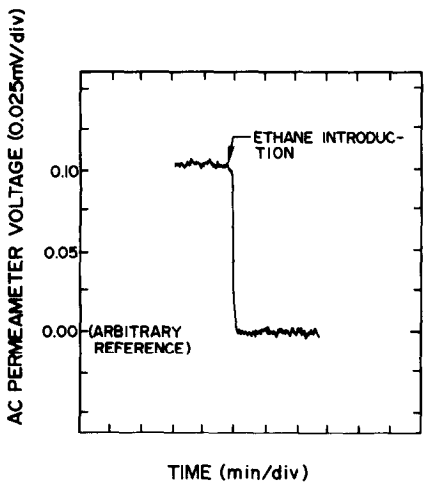

FIG. 4. Trace of a strip chart recording of ac permeameter voltage as a function of time upon initiation of hydrogenolysis.

ethane into a flow of hydrogen and helium in order to initiate hydrogenolysis. The sample remains stationary, so no sample voltage (E_s) can be determined; however, the nickel crystallite temperature before reaction initiation is that of the bulk fluid. Figure 4 is a strip chart recording of permeameter output upon introduction of ethane. Since the ethane is introduced at an essentially constant total pressure of 1 atm, there is a small decrease in hydrogen pressure. This change causes an increase in permeameter voltage; however, this is dealt with by a straightforward calibration. One of the primary reasons for studying ethane hydrogenolysis over nickel is that ethane does not affect the sample moment in the presence of significant hydrogen (*18*). The only things affecting sample voltage are crystallite temperature and hydrogen partial pressure.

Before quantitative crystallite thermometry can be performed on a given sample, two calibrations must be obtained: (1) sample voltage vs temperature at constant hydrogen pressure, and (2) sample voltage vs hydrogen pressure at constant temperature. Hydrogenolysis is performed over the nickel catalyst before these calibrations are done in order to age the sample. Otherwise, the level of carbonaceous deposits on the nickel surface may change, affecting the calibrations. As the calibrations of aged samples do not change significantly, it is apparently reasonable to assume that the level of deposits is constant.

Calibration (1) is performed in a constant flow of hydrogen. Thus, the change in nickel surface coverage by hydrogen (hence sample moment) with temperature is automatically accounted for. The sample is cyclically withdrawn and inserted into one secondary coil to obtain the sample voltage for a given temperature. Figure 5 is representative of the curves obtained; i.e., they are essentially linear over the temperature range of interest.

Calibration (2) is performed by adjusting the hydrogen partial pressure in a flow of helium and hydrogen at constant temperature. If the sample voltage at 1 atm of H_2 is used as a reference and the change in sample voltage from this is plotted, a curve like that in Figure 6 is obtained. Note that if the negative of this was plotted, a curve resembling an adsorption isotherm would result (*8, 18*). Since the change in coverage with temperature is built into the first calibration, it is sufficient to have the sample voltage vs hydrogen pressure at one temperature in the range of interest. The increase in sample voltage due to hydrogen pressure decrease, which is usually small, is added

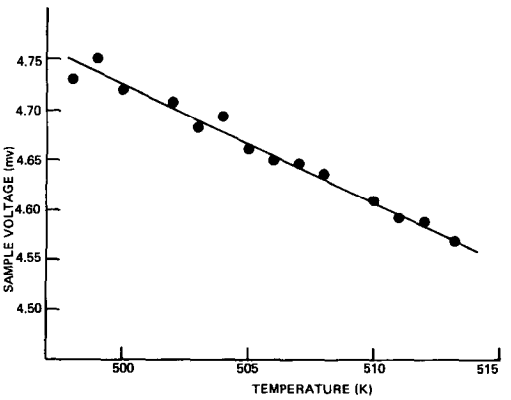

FIG. 5. Sample voltage vs temperature at constant hydrogen pressure.

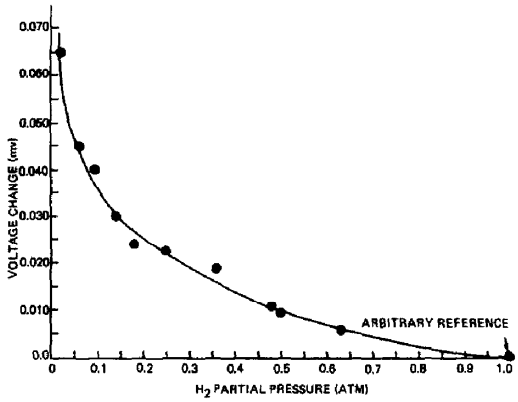

FIG. 6. Sample voltage vs hydrogen pressure at constant temperature.

to the difference in permeameter voltage before reaction initiation and after steady state is attained. A small, rapid peak sometimes occurs in the stripchart recording before the decrease in voltage due to temperature increase. This is because of the hydrogen pressure reduction (*7*), and is automatically dealt with by following the procedure above. After the total sample voltage change is determined, the average catalytic crystallite temperature is easily read off a curve similar to that of Fig. 5.

For example, the voltage change from Fig. 5 is 0.105 mV. Suppose the hydrogen pressure change is from 0.7 to 0.6 atm. Then from Fig. 6, the increase in voltage due to this decrease in hydrogen pressure is 0.003 mV. From Fig. 6, the voltage vs temperature calibration is linear for this sample with a slope of 0.012 mV/K. If the crystallite temperature before reaction initiation was 508.0 K, then it is 517.0 K after steady state is reached: (0.105 + 0.003)/0.012 = 9.0.

Currently, the temperature determined magnetically can be reproduced to within 0.2 K when the results of several experiments are averaged. Note that the correction for H_2 pressure is of the same order. Data acquisition, storage, and analysis is tedious as described. Digital data acquisition and analysis is being implemented to ease the burden, and increase reliability.

Intraparticle gradients have been ignored in the previous analysis. Even if present, partial pressure gradients would have small impact as the total corrections for hydrogen partial pressure changes are only a few percent. Internal temperature gradients are not of concern in this work, as Anderson's criterion (*19*) is satisfied by several orders of magnitude. In fact, the maximum internal temperature rise is ~0.5 K. Even in the presence of internal temperature gradients, the volumetric average temperature would be obtained.

APPLICATION AND DISCUSSION

Kinetics. The most direct application of the magnetic thermometry detailed is the determination of activation energy in the presence of external temperature gradients. Fluid to catalyst particle temperature gradients will interfere with analysis before any other gradient, as rate increases, in the usual catalytic study (20, 21). Considerable flexibility in the operating conditions of the kinetic experiments can be achieved if the average catalytic crystallite temperature is measured, as the rates can be higher before estimates of kinetic parameters will be disguised. In fact, for the ethane hydrogenolysis experiments discussed, observed rates could be an order of magnitude higher before external or internal concentration gradients cause more than 5% difference between the observed rate and the rate in the absence of these gradients. The Weisz parameter (*21*) is on the order of 10^{-2}, and Mears' criterion concerning external concentration gradients (*20*) is satisfied by an order of magnitude for the worst cases reported here. Though some slight partial pressure gradients exist, they are ignored in this work. Of course, intraparticle thermal gradients are the last to occur. As noted, Anderson's criterion (*19*) is satisfied by several orders of magnitude, and the maximum intraparticle temperature rise is conservatively estimated to be 0.5 K for the experiments performed.

The intraparticle temperature gradients

considered by Anderson (*19*) are particle scale. Catalytic crystallite to support gradients are another matter. This is an important consideration, as Sinfelt (*22*) demonstrated a crystallite size dependence on the ethane hydrogenolysis activity of nickel, though other researchers have concluded the system to be facile (*23*). These opposing results were explained by Martin (*24*), as due to differing concentrations of inactive Ni [111] planes exposed. This in turn apparently depends on preparation method and pretreatments (*24*). If crystallite to support temperature gradients are significant, then they would reasonably depend on turnover number. Hence, there would be a range of crystallite temperatures. However, in the absence of these microscopic gradients, the thermometry is unaffected by any crystallite structure dependence. It is assumed here that there are no microscopic gradients. This is apparently reasonable, at least if the time average is considered (*6*). Within the differential reactor approximation then, each crystallite in the bed is taken to have the magnetically determined temperature.

The kinetic expression for ethane hydrogenolysis can be written approximately as (*25*)

$$r = k(T)\frac{P_E}{P_{H_2}^2} \qquad (5)$$

This partial pressure dependence was used to essentially adjust all the rates to the same reference pressures. This is similar to the procedure used by Sinfelt (*25*), who reported an activation energy (E_a) for ethane hydrogenolysis over Ni/SiO_2 of 40.6 kcal/g mole (*26*). A value of 41 kcal/g mole was obtained in this laboratory using very low reaction rate data over the temperature range of 460 to 530 K. As the majority of coupled magnetic thermometry/hydrogenolysis data is in the temperature range from 500 to 520 K, attention is restricted to this range in the following.

Differential kinetic data between 0.8 and 2% were used. These limits were chosen somewhat arbitrarily. The upper limit was set for consistency in the definition of differential conversion. The lower limit was set because the scatter in the magnetically determined temperature increases rapidly below this point due to the small temperature rises. Data both failing and passing Mears' criterion dealing with external temperature gradients (*20*) are considered. A correlation suggested by Satterfield (*20*) was used to estimate the interphase heat transfer coefficient. Using the bulk stream temperature for all of the data in the conversion range considered, the activation energy is estimated to be 47 kcal/g mole. Using only the data which passes Mears' criterion, 44 kcal/g mole is estimated. Using the magnetic temperature, E_a = 41 kcal/g mole, consistent with the data taken over a wider temperature range. The effect of the 5% error allowed by Mears' criterion (*20*) is readily apparent. Of course, the effect of this is minimized if data taken over a larger temperature range is used. The reliability of the estimate made from magnetically determined temperatures would also be improved by using a wider temperature range.

Interphase transport. An application of wider interest is interphase transport as results obtained for ethane hydrogenolysis over Ni/SiO_2 should prove useful in other low Reynolds number, small particle size kinetic studies.

The use of Mears' criterion in the previous section hinges on the ability to estimate interphase transport coefficients. However, as pointed out by Satterfield (*20*), there is no reliable correlation for interphase transport coefficients in the Reynolds number range found in these experiments. It is important to note that the heat transfer and kinetic experiments are the same. The ability to measure catalytic crystallite temperature during catalysis provides the needed measure of driving force for interphase heat transfer. Remember that the catalyst particles are isothermal on a particle scale, and it is assumed that the crystallite temperature is that of the support. Within the differential reactor approx-

imation, the Nusselt number can be calculated from kinetic experiments as

$$Nu = \frac{hd_p}{k_f} = \frac{(-\Delta H)Rd_p}{a_v(T_c - T_b)k_f} \qquad (6)$$

where

h is interphase heat transport coefficient
d_p is catalyst particle diameter
k_f is reacting fluid thermal conductivity
ΔH is heat of reaction
R is observed reaction rate per catalyst volume
a_v is the external area per catalyst volume
T_c is the average crystallite temperature
T_b is the arithmetic average bulk stream temperature

Figure 7 shows some results plotted as Nusselt number vs Péclet number. Fluid properties are estimated at average reactor conditions using methods given by Reid *et al.* (*27*). These allow calculation of the Reynolds (*Re*), Prandtl (*Pr*), and hence Péclet (*Pe*) numbers. The Reynolds number ranged between 0.1 and 1.3, while Prandtl numbers only varied between 0.4 and 0.6. Thus the variation in *Pe* is due mostly to changes in *Re*, as is usual (*20*). The best fit line through the data, with a regression coefficient of 0.82, is

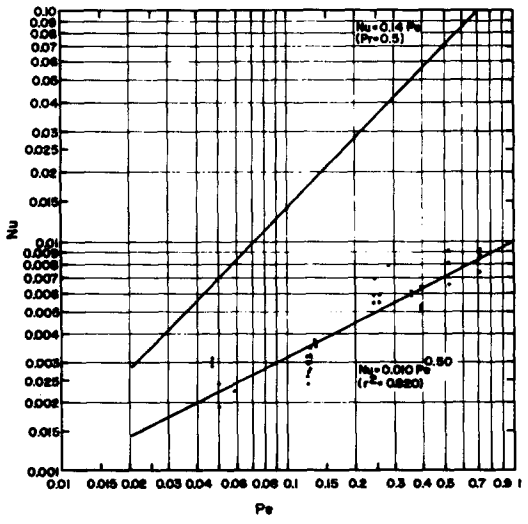

FIG. 7. Nusselt number vs Péclet number.

$$Nu = 0.010 \cdot (Pe)^{0.50} = 0.010 \cdot (Pr \cdot Re)^{0.50} \qquad (7)$$

where

Pe is $Pr \cdot Re$
Pr is $c_p\mu/k_f$
Re is $d_p\rho/\mu$
c_p is fluid heat capacity
ρ is fluid density
μ is fluid viscosity

The comments on precision in the previous section are equally valid here. It is hoped that the data scatter can be improved using digital acquisition and analysis.

The Nusselt numbers estimated in this work correspond well with past work (*28*), and the Reynolds number dependence is that found by Balakrishnan and Pei (*29*) at higher *Re* (>300). Those workers used microwave heating of the bed, so each particle had the same temperature. This eliminates conduction in the bed, which is also a reasonable assumption for a differential reactor packed with a porous catalyst having very low thermal conductivity (*20*). Equation (7) is not presented as a general correlation, since only one catalyst particle size was used (d_p = 0.16 mm). A more general correlation is currently being sought.

Also plotted in Fig. 7 is the rough guideline given by Satterfield (*20*) for the estimation of *Nu* at low Reynolds numbers. A Prandtl number of 0.5 was used for this. The Nusselt number at a given Péclet is much smaller in the present study. If the more conservative estimate of heat transfer coefficients (Eq. (7)) is used to check for external gradients, then considerably more of the hydrogenolysis kinetic data fails Mears' criterion. As noted in the previous section, this improves the estimate of activation energy.

CONCLUSION

The details of nickel crystallite thermometry were presented. It should be possible to extend the concept of the thermometry

to other systems, particularly if nickel is the catalytic metal. However, the magnetochemistry of adsorbates on cobalt and iron is not as well understood (*8*).

For systems which the thermometry can be applied to, one direct application is the determination of activation energy in the presence of external temperature gradients. An application of wider interest is the determination of interphase heat transport coefficients. Once a correlation is established, it should be applicable to other systems. Work is underway to explain the large differences between theoretical and empirical Nusselt numbers at low Reynolds numbers.

ACKNOWLEDGMENTS

Financial support from the National Science Foundation and the Petroleum Research Fund is gratefully acknowledged.

REFERENCES

1. Luss, D., *J. Chem. Eng.* **1,** 311 (1970).
2. Ruckenstein, E., and Petty, C. A., *Chem. Eng. Sci.* **27,** 937 (1972).
3. Chan, S. H., Low, M. J. D., and Mueller, W. K., *AIChE J.* **17**(6), 1499 (1971).
4. Wei, J., *Chem. Eng. Sci.* **21,** 1171 (1966).
5. Steinbruchel, C. H., and Schmidt, L. D., *Surf. Sci.* **40,** 693 (1973).
6. Holstein, W. L., and Bondart, M., *Rev. Latinoamer. Ing. Quim. Quim. Apl.* **13**(2), 107 (1983).
7. Cale, T. S., and Ludlow, D. K., *J. Catal.* **86**(2), 450 (1984).
8. Selwood, P. W., "Chemisorption and Magnetization." Academic Press, New York, 1975.
9. Cale, T. S., Ph.D. dissertation, University of Houston, Texas, 1980.
10. Cale, T. S., and Richardson, J. T., *J. Catal.* **79,** 378 (1983).
11. Cale, T. S., Richardson, J. T., and Ginestra, J., *Appl. Phys. Lett.* **42**(8), 744 (1983).
12. Van Dillen, J. A., Geus, J. W., Hermans, L. A. M., and van der Meijden, J., "Proceedings, 6th International Congress on Catalysis," p. 677. Elsevier, Amsterdam, 1976.
13. Richardson, J. T., Dubus, R. J., Crump, J. G., Desai, P., Ostewalder, U., and Cale, T. S., *in* "Preparation of Catalysts II" (B. Delmon, P. Grange, P. Jacobs, and G. Poncelet, Eds.). Elsevier, Amsterdam, 1978.
14. Dubus, M. S. thesis, University of Houston, Texas, 1977.
15. United Technologies Essex Group, Fort Wayne, Ind.
16. Richardson, J. T., *J. Catal.* **21**(1), 130 (1971).
17. Martin, G. A., Dutarte, R., and Dalmon, J. A., *in* "Growth and Properties of Metal Clusters" (J. Bourdon, Ed.), p. 467. Elsevier, Amsterdam.
18. Martin, G. A., and Imelik, B., *Surf. Sci.* **42,** 157 (1974).
19. Anderson, J. B., *Chem. Eng. Sci. 18,* 147 (1963).
20. Satterfield, C. N., "Heterogeneous Catalysis in Practice." McGraw–Hill, New York, 1980.
21. Froment, G. F., and Bischoff, K. B., "Chemical Reactor Analysis and Design." Wiley, New York, 1979.
22. Carter, J. L., Cusumano, J. A., and Sinfelt, J. H., *J. Amer. Chem. Soc.* **70**(7), 2257 (1966).
23. Rhydin, Y. A., Kuznetsov, B. N., and Yermakov, Y. I., *React. Kinet. Catal. Lett.* **7,** 105 (1977).
24. Martin, G. A., *J. Catal.* **60,** 452 (1979).
25. Sinfelt, J. H., Carter, J. L., and Yates, D. J. C., *J. Catal.* **24,** 283 (1972).
26. Sinfelt, J. H., Taylor, W. F., and Yates, D. J. C., *J. Phys. Chem.* **68,** 2962 (1964).
27. Reid, R. C., Prausnitz, J. M., and Sherwood, T. K., "The Properties of Gases and Liquids." McGraw–Hill, New York, 1977.
28. Martin, H., *Chem. Eng. Sci.* **33,** 913 (1978).
29. Balakrishnan, A. R., and Pei, D. C. T., *Ind. Eng. Chem. Proc. Des. Dev.* **18**(1), 30 (1979).